Mode Evolution of Cyclic Symmetric Rotors Assembled to Flexible Bearings and Housing

Hyunchul Kim
Graduate Student

Nick Theodore Khalid Colonnese
Undergraduate Student

I. Y. Shen[1]
Professor
e-mail: ishen@u.washington.edu

Department of Mechanical Engineering,
University of Washington,
Box 352600 Seattle, WA 98195-2600

*This paper is to study how the vibration modes of a cyclic symmetric rotor evolve when it is assembled to a flexible housing via multiple bearing supports. Prior to assembly, the vibration modes of the rotor are classified as "balanced modes" and "unbalanced modes." Balanced modes are those modes whose natural frequencies and mode shapes remain unchanged after the rotor is assembled to the housing via bearings. Otherwise, the vibration modes are classified as unbalanced modes. By applying fundamental theorems of continuum mechanics, we conclude that balanced modes will present vanishing inertia forces and moments as they vibrate. Since each vibration mode of a cyclic symmetric rotor can be characterized in terms of a phase index (Chang and Wickert, "Response of Modulated Doublet Modes to Travelling Wave Excitation," J. Sound Vib., **242**, pp. 69–83; Chang and Wickert, 2002, "Measurement and Analysis of Modulated Doublet Mode Response in Mock Bladed Disks," J. Sound Vib., **250**, pp. 379–400; Kim and Shen, 2009, "Ground-Based Vibration Response of a Spinning Cyclic Symmetric Rotor With Gyroscopic and Centrifugal Softening Effects," ASME J. Vibr. Acoust. (in press)), the criterion of vanishing inertia forces and moments implies that the phase index by itself can uniquely determine whether or not a vibration mode is a balanced mode as follows. Let N be the order of cyclic symmetry of the rotor and n be the phase index of a vibration mode. Vanishing inertia forces and moments indicate that a vibration mode will be a balanced mode if $n \neq 1, N-1, N$. When $n = N$, the vibration mode will be balanced if its leading Fourier coefficient vanishes. To validate the mathematical predictions, modal testing was conducted on a disk with four pairs of brackets mounted on an air-bearing spindle and a fluid-dynamic bearing spindle at various spin speeds. Measured Campbell diagrams agree well with the theoretical predictions.* [DOI: 10.1115/1.3147167]

1 Introduction

Rotary machines appear in many industrial sectors and have wide applications from jet engines to compressors. Every rotary machine consists of three major components: a rotating part (rotor), a stationary part (housing), and multiple bearings connecting the rotor and the housing. For many rotary machines, the rotors are cyclic symmetric. Some examples are turbine disks, compressor blades, and propellers.

For many industries that employ rotary machines, the ability to accurately predict rotor response is critical for several reasons. First, it can significantly shorten design cycles and reduce costs. Second, it can significantly enhance rotor performance. Third, it can lead to model-based health monitoring systems that enable early detection of rotor failures enhancing rotor reliability. Traditionally, vibration analysis of spinning cyclic symmetric rotors adopts a set of rotor-based coordinates [1–8]. The advantage is that the governing equations of the spinning rotors have constant coefficients; therefore, rotor-based responses are reasonably easy to obtain.

Recently, rapid industrial developments demand accurate predictions of ground-based vibration responses of spinning cyclic symmetric rotors [9]. This is especially true when the spinning rotors are coupled with a stationary housing via multiple bearings. For example, with increased material and energy costs, the turbine engine industry seeks to reduce the weight and thus the rigidity of turbine engines. This results in significant vibration coupling the rotor, bearings, and housing. With increased maintenance costs, turbine engine industry seeks to monitor engine health to replace routine maintenance. In particular, monitoring engine health via the stationary housing will require no sensors attached to the spinning rotor thus avoiding issues such as unbalance and poor reliability.

The presence of the housing and bearings affects the vibration of a spinning cyclic symmetric rotor in many ways. Phenomenally, when a rotor is assembled to a housing via a set of bearings, some vibration modes of the rotor may not be coupled to the housing. In other words, these vibration modes do not "sense" the existence of the housing and the bearings. Therefore, the presence of the bearings and housing will not alter natural frequencies and mode shapes of these vibration modes. These modes are defined as balanced modes in this paper. In contrast, unbalanced modes refer to those vibration modes that become coupled to the housing via the bearing after assembly. The unbalanced modes "sense" the existence of the housing and bearings, and will alter their natural frequencies and mode shapes after the rotor is assembled to the housing via the bearing.

The phenomenon of balanced and unbalanced modes and their coupling with bearings and housings have been known for rotors with specific geometries, such as circular disks. For example, Shen and Ku [10] studied the vibration of spinning multiple disks mounted on a rigid spindle supported by a pair of ball bearings. According to Ref. [10], balanced modes can appear in several forms for a disk-spindle system. For example, disk vibration modes with two or more nodal diameters are balanced modes. Also, if two disks experience out-of-phase vibration in either one-nodal-diameter or zero-nodal-diameter modes while other disks experience no vibration, these modes are balanced modes. For these balanced modes, their natural frequencies and mode shapes

[1]Corresponding author.

Contributed by the Technical Committee on Vibration and Sound of ASME for publication in the JOURNAL OF VIBRATION AND ACOUSTICS. Manuscript received January 20, 2009; final manuscript received March 27, 2009; published online September 11, 2009. Assoc. Editor: Jiong Tang. Paper presented at the 2009 Biennial Conference on Mechanical Vibration and Noise.

Downloaded 11 Sep 2009 to 128.12.241.41. Redistribution subject to ASME license or copyright; see http://www.asme.org/terms/Terms_Use.cfm

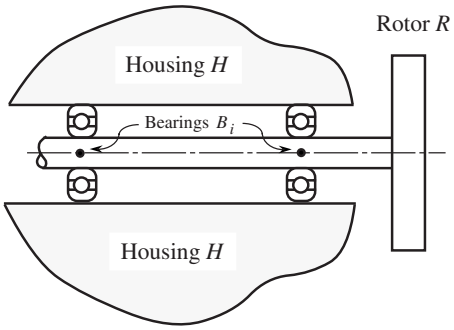

Fig. 1 An asymmetric rotor supported by a stationary housing via bearings

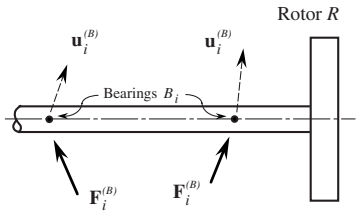

Fig. 2 Free-body diagram of the rotor after it is assembled to a housing via bearings

remain unchanged when the disk-spindle assembly is mounted onto a pair of bearings. In contrast, if all the disks experience in-phase vibration in one-nodal-diameter or zero-nodal-diameter modes, they are unbalanced modes and their natural frequencies can be significantly reduced when the bearings are present.

Mathematically, when an asymmetric or a cyclic symmetric rotor is assembled to a housing via a set of bearings, the governing equations of motion do not have constant coefficients. Instead, they have periodic coefficients with the spin speed ω_3 being the fundamental frequency. For example, many researchers have studied vibration and instability of spinning asymmetric shafts [11–18]. In these studies, the rotor takes the form of a slender shaft with asymmetric cross section. Since the equation of motion appears as a set of ordinary differential equations with periodic coefficients, instability occurs in the form of parametric resonances. Given that the coefficients are not constant, numerical solutions of the governing equations are computationally intensive as the number of degrees of freedom increases.

Under these circumstances, balanced modes can effectively reduce the order of the governing equation. Since balanced modes are not coupled to the housing, their response can be solved through the traditional rotor-based analysis, whose equations of motion have constant coefficients. In contrast, the unbalanced modes are coupled to the housing; therefore, the equations of motion governing the unbalanced modes will have periodic coefficients. By separating the balanced and unbalanced modes, one can effectively reduce the order of the ordinary differential equation with periodic coefficients to reduce computational efforts.

With the explanation above, it is critical to identify balance modes and unbalanced modes for phenomenal and computational reasons. Nevertheless, rigorous and easy-to-use criteria to distinguish balanced and unbalanced modes remain open thus far.

The purpose of this paper is to develop several rigorous yet easy-to-use criteria to distinguish balanced and unbalanced modes for cyclic symmetric rotors. We first apply fundamental theorems in continuum mechanics to show that balanced modes must have vanishing inertia forces and moments as they vibrate, which, in turn, leads to the following two criteria to identify balanced modes. The first criterion is vanishing boundary nodal forces and moments. The second criterion is via phase index of a cyclic symmetric rotor. Finally, calibrated experiments and finite element simulations are then conducted on circular disks with four pairs of evenly spaced brackets to verify the mathematical criteria.

2 Mathematical Formulations

Figure 1 symbolically shows a rotor R attached to a stationary housing H via multiple bearings B_i, $i=1,2,\ldots,n_b$, where n_b is the number of bearings. Moreover, the bearings B_i are assumed to be point contacts. Figure 2 shows the free-body diagram of the rotor. Note that the bearing forces $\mathbf{F}_i^{(B)}$, $i=1,2,\ldots,n_b$, acting on the rotor R replace the effect of the stationary housing. For a balanced mode, the presence of the stationary housing H does not affect the rotor R. This implies that no forces are transmitted through the bearings. In other words, the bearing forces must vanish no matter how the rotor is supported at the bearings, that is,

$$\mathbf{F}_i^{(B)}(\mathbf{r}) = \mathbf{0}, \quad i = 1,2,\ldots,n_b \tag{1}$$

The physical meaning of Eq. (1) is that the inertia force and inertia moment of the rotor R must vanish for a balanced mode, no matter how the rotor is supported at the bearings. According to continuum mechanics, free vibration of the rotor prior to assembly satisfies

$$\sigma_{ij,j} = \rho \ddot{u}_i, \quad i = 1,2,3 \tag{2}$$

where σ_{ij} are stress components, u_i are displacement components, and ρ is the density of the rotor. In Eq. (2), traditional tensor notations are used, i.e., 1, 2, and 3 represent the three orthogonal coordinates, commas represent spatial derivatives, and repeated indices mean summation from 1 to 3. Integration of Eq. (2) over the rotor volume R and the application of the divergence theorem results in

$$\int_R \rho \ddot{u}_i dV = \int_R \sigma_{ij,j} dV = \int_{\partial R} \sigma_{ij} n_j dS, \quad i = 1,2,3 \tag{3}$$

where ∂R is the surface of rotor R, and n_j is the surface outer normal. According to Eq. (1), zero bearing forces imply that $\sigma_{ij} n_j = 0$. Therefore, the rotor R must experience zero inertia force.

$$\int_R \rho \ddot{u}_i dV = 0, \quad i = 1,2,3 \tag{4}$$

for a balanced mode, no matter how the rotor is supported at the bearings. Similarly, one can follow established theorems in continuum mechanics to show that the rotor R must experience zero inertia moment.

$$\int_R \rho e_{kji} x_j \ddot{u}_i dV = \int_R e_{kji} x_j \sigma_{ip,p} dV = \int_{\partial R} e_{kji} x_j \sigma_{ip} n_p dV = 0, \quad k = 1,2,3 \tag{5}$$

where e_{kji} is the permutation symbol and x_j, $j=1,2,3$, are the coordinates of the position vector. The assumption of symmetric stress components σ_{ij} are also used in deriving Eq. (5).

Let us consider the case where the balanced mode of interest has a nonzero natural frequency ω with mode shape $\mathbf{w}(\mathbf{r})$, where $\mathbf{r}$ is the position vector. Therefore, $(u_1,u_2,u_3)^T = \mathbf{w}(\mathbf{r})e^{j\omega t}$, and Eqs. (4) and (5) become

$$\int_R \rho \mathbf{w}(\mathbf{r}) dV = \int_R \rho \mathbf{r} \times \mathbf{w}(\mathbf{r}) dV = \mathbf{0} \tag{6}$$

3 Criterion 1: Boundary Forces

For many practical applications, the rotor R often consists of a very rigid portion and a relatively flexible portion. Moreover, the bearings are attached to the very rigid portion. For example, disk drive spindle motors consist of multiple flexible disks mounted on

Downloaded 11 Sep 2009 to 128.12.241.41. Redistribution subject to ASME license or copyright; see http://www.asme.org/terms/Terms_Use.cfm

a fairly rigid hub. In addition, the rigid hub is connected to the stationary housing via bearings. When a rigid portion appears in a rotor, existence of balanced modes can be detected by analyzing the vibration of the flexible portion alone as follows.

Let us denote the rigid portion of the rotor as R_r and the flexible portion of the rotor as R_f. Also, let I be the interface between the rigid portion R_r and the flexible portion R_f. In addition, the bearings are located at some finite points of the rigid portion R_r.

Since the rotor R can be subjected to any boundary conditions at the bearings, let us assume that the rotor R is subjected to a fixed boundary condition at the bearings prior to assembly to a housing. Since the rigid portion R_r is subjected to the fixed boundary condition, R_r will not contribute to the inertia force. Nevertheless, the flexible portion R_f of the rotor still satisfies the governing equation of motion in continuum mechanics. Therefore, Eq. (4) leads to

$$\int_R \rho \ddot{u}_i dV = \int_{R_f} \rho \ddot{u}_i dV = \int_{R_f} \sigma_{ij,j} dV = 0, \quad i = 1,2,3 \tag{7}$$

Application of divergence theorem to Eq. (7) results in

$$\int_R \rho \ddot{u}_i dV = \int_I \sigma_{ij} n_j dS = 0, \quad i = 1,2,3 \tag{8}$$

Similarly, Eq. (5) implies that

$$\int_R \rho e_{kji} x_j \ddot{u}_i dV = \int_{R_f} \rho e_{kji} x_j \ddot{u}_i dV = \int_I e_{kji} x_j \sigma_{ip} n_p dS = 0, \quad k = 1,2,3 \tag{9}$$

Equations (8) and (9) imply that integrated tractions in terms of forces and moments must vanish at the interface I for a balanced mode.

This criterion is easy to use especially in combination with finite element analyses. For each vibration mode, let $\mathbf{F}^{(I)}$ and $\mathbf{M}^{(I)}$ be the nodal forces and moments at the interface I obtained from a finite element analysis. Then the vanishing surface integrals in Eqs. (8) and (9) imply that

$$\sum_j \mathbf{F} = \sum_j [\mathbf{M}^{(I)} + \mathbf{r}^{(I)} \times \mathbf{F}^{(I)}] = \mathbf{0} \tag{10}$$

where $\mathbf{r}^{(I)}$ is the position vector of the nodes located on the interface I, and the summation is over all the nodes on the interface I.

4 Criterion 2: Phase Index

Let us consider a stationary cyclic symmetric rotor of order N. The rotor consists of N identical substructures $S^{(i)}$, $i=1,2,\ldots,N$, and each substructure spans an angle of $2\pi/N$. According to Ref. [9], vibration modes of a stationary cyclic symmetric rotor have the following properties of interests for identifying balanced and unbalanced modes.

First, the mode shapes have periodicity. Let us consider a vibration mode shape $\mathbf{W}(\tilde{\mathbf{r}})$, which can be complex. In addition, let us define the mode shape at the ith substructure as $\mathbf{W}^{(i)}(\tilde{\mathbf{r}})$, so that

$$\mathbf{W}(\tilde{\mathbf{r}}) \equiv \mathbf{W}^{(1)}(\tilde{\mathbf{r}}) \cup \mathbf{W}^{(2)}(\tilde{\mathbf{r}}) \cup \ \ldots \ \cup \mathbf{W}^{(N)}(\tilde{\mathbf{r}}) \tag{11}$$

As a result of the cyclic symmetry, the mode shapes at two neighboring substructures must differ by a constant phase, that is,

$$\mathbf{W}^{(i+1)}(\tilde{\mathbf{r}}) = \mathbf{W}^{(i)}(\tilde{\mathbf{r}}) e^{j2\pi n/N} \tag{12}$$

where $j \equiv \sqrt{-1}$ and $n \in (1,2,\ldots,N)$. In this paper, n is defined as the *phase index* of the vibration mode. The phase index, usually, can be identified through Eq. (12), if explicit mode shapes are available. The phase index n is also known as the circumferential wave number or the phase parameter in the literature. In order for the phase index n to work, the mode shapes in Eq. (12) are generally complex, because the exponent $j2\pi n/N$ is a pure imaginary number.

The second property is mode shape modulation. Specifically, mode shape $\mathbf{W}(\tilde{\mathbf{r}})$ is periodic in the circumferential (i.e., θ) direction and can be expanded in terms of the following Fourier series [9]:

$$\mathbf{W}(\tilde{\mathbf{r}}) = \sum_{k=n+\mathbf{M}(N)} \mathbf{A}_k(r,z) e^{jk\theta} \tag{13}$$

where $\mathbf{M}(N)$ denotes an integer multiple of N and

$$\mathbf{A}_k(r,z) = \frac{N}{2\pi} \int_0^{2\pi/N} e^{-jk\theta} \mathbf{W}^{(1)}(r,z,\theta) d\theta \tag{14}$$

In order for the mode shape $\mathbf{W}(\tilde{\mathbf{r}})$ to be a balanced mode, the vibration mode must have vanishing inertia forces and moments as shown in Eq. (6). If the rotor is made of a homogenous material, the density is constant. Therefore, vanishing inertia forces (6) implies that

$$\int \mathbf{W}(\tilde{\mathbf{r}}) dV = \sum_{k=n+\mathbf{M}(N)} \int \mathbf{A}_k(r,z) dA \int_0^{2\pi} e^{jk\theta} d\theta = \begin{cases} 0, & n \neq N \\ 2\pi \int \mathbf{A}_0(r,z) dA, & n = N \end{cases} \tag{15}$$

For the case $n=N$, $\int \mathbf{W}(\tilde{\mathbf{r}}) dV$ may or may not be zero depending on the explicit expression of $\mathbf{A}_0(r,z)$.

Similarly, vanishing inertia moments (6) require that

$$\int \tilde{\mathbf{r}} \times \mathbf{W}(\tilde{\mathbf{r}}) dV = 0 \tag{16}$$

where $\tilde{\mathbf{r}}$ is a position vector. In polar coordinates, the position vector is

$$\tilde{\mathbf{r}} = r \cos\theta \mathbf{e}_x + r \sin\theta \mathbf{e}_y + z\mathbf{e}_z = \mathbf{b}(r) e^{j\theta} + \mathbf{b}^*(r) e^{-j\theta} + z\mathbf{e}_z \tag{17}$$

where $\mathbf{e}_x$, $\mathbf{e}_y$, and $\mathbf{e}_z$ are unit vectors along the x, y, and z axes,[2] the superscript $(*)$ represents a complex conjugate, and

$$\mathbf{b}(r) \equiv \frac{r}{2}(\mathbf{e}_x - j\mathbf{e}_y) \tag{18}$$

Substitution of Eqs. (13) and (17) in Eq. (16) results in

$$\int \tilde{\mathbf{r}} \times \mathbf{W}(\tilde{\mathbf{r}}) dV = S_1 + S_2 + S_3 \tag{19}$$

where

$$S_1 \equiv \sum_{k=n+\mathbf{M}(N)} \int [\mathbf{b}(r) \times \mathbf{A}_k(r,z)] dA \int_0^{2\pi} e^{j(k+1)\theta} d\theta = \begin{cases} 2\pi \int [\mathbf{b}(r) \times \mathbf{A}_{-1}(r,z)] dA, & n = N-1 \\ 0, & n \neq N-1 \end{cases} \tag{20}$$

$$S_2 \equiv \sum_{k=n+\mathbf{M}(N)} \int [\mathbf{b}^*(r) \times \mathbf{A}_k(r,z)] dA \int_0^{2\pi} e^{j(k-1)\theta} d\theta = \begin{cases} 2\pi \int [\mathbf{b}^*(r) \times \mathbf{A}_1(r,z)] dA, & n = 1 \\ 0, & n \neq 1 \end{cases} \tag{21}$$

[2]The z axis is assumed to be the spin axis.

Downloaded 11 Sep 2009 to 128.12.241.41. Redistribution subject to ASME license or copyright; see http://www.asme.org/terms/Terms_Use.cfm

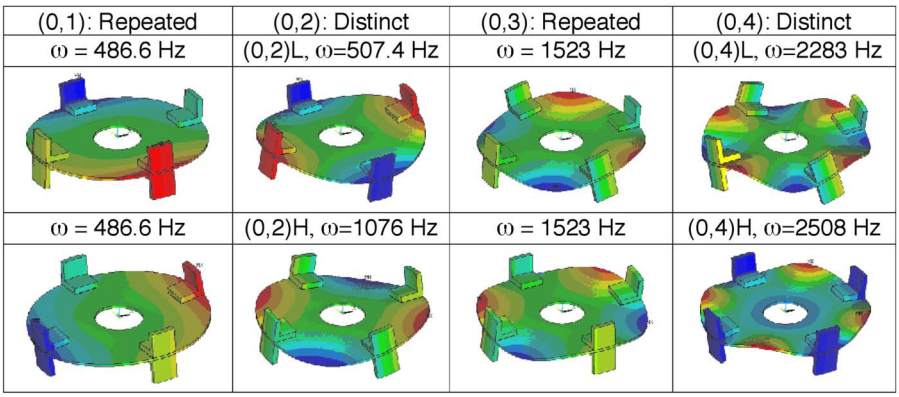

Fig. 3 Mode shapes of a circular disk with four pairs of brackets; low-frequency range

$$S_3 \equiv \sum_{k=n+\mathbf{M}(N)} \int [z\mathbf{e}_z \times \mathbf{A}_k(r,z)]dA \int_0^{2\pi} e^{jk\theta} d\theta = \begin{cases} 2\pi \int [z\mathbf{e}_z \times \mathbf{A}_0(r,z)]dA, & n = N \\ 0, & n \neq N \end{cases} \tag{22}$$

According to Eqs. (20)–(22),

$$\int \tilde{\mathbf{r}} \times \mathbf{W}(\tilde{\mathbf{r}})dV = 0, \quad n \neq 1, N-1, N \tag{23}$$

Otherwise, whether $\int \tilde{\mathbf{r}} \times \mathbf{W}(\tilde{\mathbf{r}})dV$ is zero will depend on the explicit expression of $\mathbf{A}_0(r,z)$, $\mathbf{A}_1(r,z)$, and $\mathbf{A}_{-1}(r,z)$.

Based on the discussions above, a vibration mode with phase index n satisfying

$$n \neq 1, N-1, N \tag{24}$$

will be a balanced mode. Otherwise, the vibration mode may or may not be a balanced mode depending on the explicit expression of $\mathbf{A}_0(r,z)$, $\mathbf{A}_1(r,z)$, and $\mathbf{A}_{-1}(r,z)$.

Equation (24) has two significant consequences. First, if a cyclic symmetric rotor has a twofold or threefold geometry (i.e., $N=2$ or $N=3$), all vibration modes are unbalanced. Second, if a cyclic symmetric rotor has large N (e.g., turbine disks), most of the modes will be balanced.

5 Numerical Studies

In the numerical studies, let us consider a circular disk with four pairs of brackets that are evenly spaced in the circumferential directions. Moreover, the inner rim of the circular disk is fixed to simulate the condition of a rigid hub. A finite element analysis is conducted first to calculate natural frequencies, mode shapes, and nodal forces and moments at the inner rim for each vibration mode. Then Eqs. (10) and (24) are used to check whether or not a vibration mode is a balanced mode. The results are explained as follows.

Figure 3 shows the natural frequencies and mode shapes at the low-frequency range. When the brackets are not present, the circular disk is axisymmetric with its vibration mode shapes characterized by (m,n), where m and n refer to the numbers of nodal circles and nodal diameters, respectively. Moreover, vibration modes with one or more nodal diameters have repeated natural frequencies. As Fig. 3 indicates, the presence of the brackets causes some of the repeated modes to split into modes with distinct frequencies. At the low-frequency range, the (m,n) notation for nodal circles and nodal diameters work relatively well. According to Fig. 3, (0,1) and (0,3) modes remain repeated, whereas (0,2) and (0,4) modes become split with distinct frequencies. For those modes with distinct frequencies, the notations L and H refer to vibration modes with the low and high frequencies, respectively.

Figure 4 shows natural frequencies and mode shapes at the high-frequency range. We note that these mode shapes do not present clear nodal diameters as in the low-frequency modes. Therefore, we will not use the (m,n) notation. Instead, we will simply refer to them as 10th or 11th modes and so on for simplicity. The numerical results show that 10th and 11th modes are repeated, 12th and 13th modes are distinct, and 14th and 15th modes are repeated.

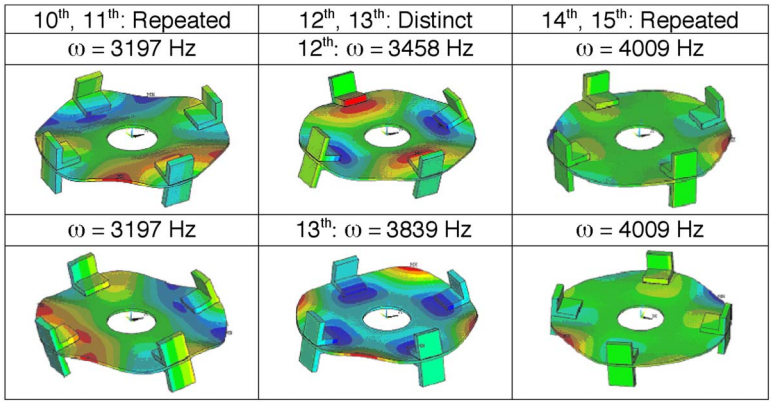

Fig. 4 Mode shapes of a circular disk with four pairs of brackets; high-frequency range

Downloaded 11 Sep 2009 to 128.12.241.41. Redistribution subject to ASME license or copyright; see http://www.asme.org/terms/Terms_Use.cfm

Table 1 Nodal forces and moments for the circular disk with four pairs of brackets

Mode	ΣF_x	ΣF_y	ΣF_z	ΣM_x	ΣM_y	Type
(0,1)	$-1.08\times10^{+00}$	5.28×10^{-01}	$-8.79\times10^{+00}$	$3.99\times10^{+07}$	$3.37\times10^{+07}$	Unbalanced
(0,1)	1.45×10^{-01}	-7.46×10^{-01}	$-1.43\times10^{+01}$	$3.37\times10^{+07}$	$-3.99\times10^{+07}$	Unbalanced
(0,0)	-4.70×10^{-01}	-9.39×10^{-01}	$-1.83\times10^{+06}$	$-2.56\times10^{+02}$	$-2.54\times10^{+01}$	Unbalanced
(0,2)L	-7.31×10^{-01}	$3.69\times10^{+00}$	$-2.54\times10^{+01}$	$-1.11\times10^{+01}$	$1.02\times10^{+02}$	Balanced
(0,2)H	$-8.73\times10^{+00}$	$-3.96\times10^{+00}$	$-3.36\times10^{+01}$	$5.27\times10^{+02}$	$-2.44\times10^{+02}$	Balanced
(0,3)	$6.99\times10^{+00}$	$-1.88\times10^{+00}$	$-2.22\times10^{+00}$	$7.62\times10^{+07}$	$-6.85\times10^{+07}$	Unbalanced
(0,3)	$1.59\times10^{+00}$	$-2.21\times10^{+01}$	$9.60\times10^{+00}$	$-6.85\times10^{+07}$	$-7.62\times10^{+07}$	Unbalanced
(0,4)L	$-3.13\times10^{+01}$	$7.45\times10^{+00}$	$8.86\times10^{+01}$	$-3.32\times10^{+02}$	$-1.02\times10^{+02}$	Balanced
(0,4)H	$2.05\times10^{+01}$	$1.53\times10^{+01}$	$-1.53\times10^{+07}$	$-5.31\times10^{+02}$	$1.07\times10^{+03}$	Unbalanced
10th	$-2.00\times10^{+00}$	$-4.39\times10^{+00}$	$2.47\times10^{+01}$	$-1.70\times10^{+06}$	$-3.43\times10^{+08}$	Unbalanced
11th	$1.07\times10^{+01}$	$-9.67\times10^{+01}$	$8.14\times10^{+01}$	$3.43\times10^{+08}$	$-1.70\times10^{+06}$	Unbalanced
12th	$-9.01\times10^{+00}$	$1.16\times10^{+02}$	$-7.47\times10^{+02}$	$-9.58\times10^{+03}$	$-8.99\times10^{+03}$	Balanced
13th	$1.01\times10^{+02}$	$1.94\times10^{+01}$	$3.06\times10^{+07}$	$3.66\times10^{+03}$	$-7.03\times10^{+03}$	Unbalanced
14th	$1.31\times10^{+01}$	$3.10\times10^{+01}$	$5.14\times10^{+02}$	$9.26\times10^{+07}$	$3.24\times10^{+08}$	Unbalanced
15th	$-4.56\times10^{+00}$	$-7.89\times10^{+01}$	$1.37\times10^{+03}$	$-3.24\times10^{+08}$	$9.26\times10^{+07}$	Unbalanced

Table 1 lists the sum of nodal forces and moments of the disk-bracket rotor at the inner rim. Since the mode shapes are normalized with respect to the mass matrix of the disk-bracket rotor, the absolute value of the nodal forces and moment at the inner rim does not have much meaning. Instead, the relative value is more important. According to Table 1, nodal forces and moments of (0,2)L, (0,2)H, (0,4)L, and 12th modes are at least three or four orders-of-magnitude smaller than those of the other modes. Therefore, (0,2)L, (0,2)H, (0,4)L, and 12th modes are balanced modes due to their much lower nodal forces and moments at the inner rim relative to other modes.

Table 2 lists the phase index of the vibration modes of the disk-bracket system obtained from Ref. [9]. There are several things worth noting. First, the disk-bracket system consists of four identical substructures. Therefore, the periodicity or order of the system is $N=4$ and the phase index n ranges from 1 to 4. Second, when the phase index n is 2 or 4, Eq. (12) indicates that the mode shapes are real. In contrast, the phase index $n=1$ or $n=3$ can only be realized via complex modes. This can only be achieved through the use of a pair of repeated modes by linearly combining their mode shapes via complex coefficients. Hence, the repeated modes in Table 2 all contribute to complex modes with phase index either $n=1$ or $n=3$. Third, when the phase index $n=4$, $\mathbf{A}_0(r,z)$ is zero for (0,4)L mode and the 12th mode [9].

According to Eq. (24), a vibration mode will be a balance mode if its phase index n satisfies $n\neq1,3,4$. Therefore, (0,2)L and (0,2)H modes with $n=2$ are balanced modes. In addition, for those vibration modes with $n=4$ and $\mathbf{A}_0(r,z)=0$, Eqs. (15) and (22) lead to $\int\mathbf{W}(\tilde{\mathbf{r}})dV=\int\tilde{\mathbf{r}}\times\mathbf{W}(\tilde{\mathbf{r}})dV=\mathbf{0}$. As a result, (0,4)L and 12th modes are balanced according to Table 2. These results are consistent with those obtained through vanishing nodal forces and moments at the inner rim as predicted in Table 1.

Table 2 Phase index of the circular disk with four pairs of brackets

Mode	Phase index n	Type	Comments
(0,1)	1,3	Unbalanced	
(0,1)	1,3	Unbalanced	
(0,0)	4	Unbalanced	$\mathbf{A}_0(r,z)\neq0$
(0,2)L	2	Balanced	
(0,2)H	2	Balanced	
(0,3)	1,3	Unbalanced	
(0,3)	1,3	Unbalanced	
(0,4)L	4	Balanced	$\mathbf{A}_0(r,z)=0$
(0,4)H	4	Unbalanced	$\mathbf{A}_0(r,z)\neq0$
10th	1,3	Unbalanced	
11th	1,3	Unbalanced	
12th	2	Balanced	$\mathbf{A}_0(r,z)=0$
13th	4	Unbalanced	$\mathbf{A}_0(r,z)\neq0$
14th	1,3	Unbalanced	
15th	1,3	Unbalanced	

6 Experimental Studies

Calibrated experiments have also been conducted to validate the predictions of balanced modes for the circular disk with 4 pairs of brackets. The experiments include a stationary test and a spinning test. They are explained in detail as follows.

6.1 Stationary Test. Figure 5 shows the experimental setup. Basically, a disk-bracket specimen is first clamped onto a rigid hub support (see Fig. 6(*a*) for a blowup). An automatic hammer excites the disk-bracket specimen, and a load cell at the tip of the hammer measures the force input to the specimen. In the meantime, a laser Doppler vibrometer (LDV) measures the velocity of the specimen. Both the force and velocity measurements are fed into a spectrum analyzer to calculate a frequency response function. The experiment is then repeated for various hammer tapping locations. Natural frequencies and mode shapes are then extracted from the measured frequency response functions.

Upon identifying the natural frequencies and mode shapes of the disk-bracket specimen on the rigid hub support, the specimen is then transferred to a ball-bearing spindle motor (Fig. 6(*b*)) and a fluid-dynamic bearing spindle motor (Fig. 6(*c*)), where the same experiment is repeated to measure natural frequencies and mode shapes. In all three rounds of the experiments, the same clamp and spacers are used. Also, the clamping torque of each screw is maintained at 0.35 N m to ensure that the disk-bracket specimen receives the same boundary condition for all three setups.

According to the theory developed in this paper, a balanced mode as predicted in Tables 1 and 2 shall not change its natural frequency regardless of the types of the housings and bearings. In contrast, the unbalanced modes will behave otherwise.

Table 3 compares the natural frequencies measured from the stationary test using the three spindle setups. The first column of Table 3 refers to the vibration modes illustrated in Figs. 3 and 4. The second, third, and fourth columns of Table 3 refer to natural frequencies measured from the rigid hub support, ball-bearing spindle (BBS) motor and fluid-bearing spindle (FBS) motor, respectively. Note that some of the modes become overdamped and cannot be observed, when the rotor is mounted on the FBS motor due to significant damping from the fluid bearings. The fifth and sixth columns refer to the percent changes of the natural frequencies from the rigid hub support for the cases of the ball-bearing

Downloaded 11 Sep 2009 to 128.12.241.41. Redistribution subject to ASME license or copyright; see http://www.asme.org/terms/Terms_Use.cfm

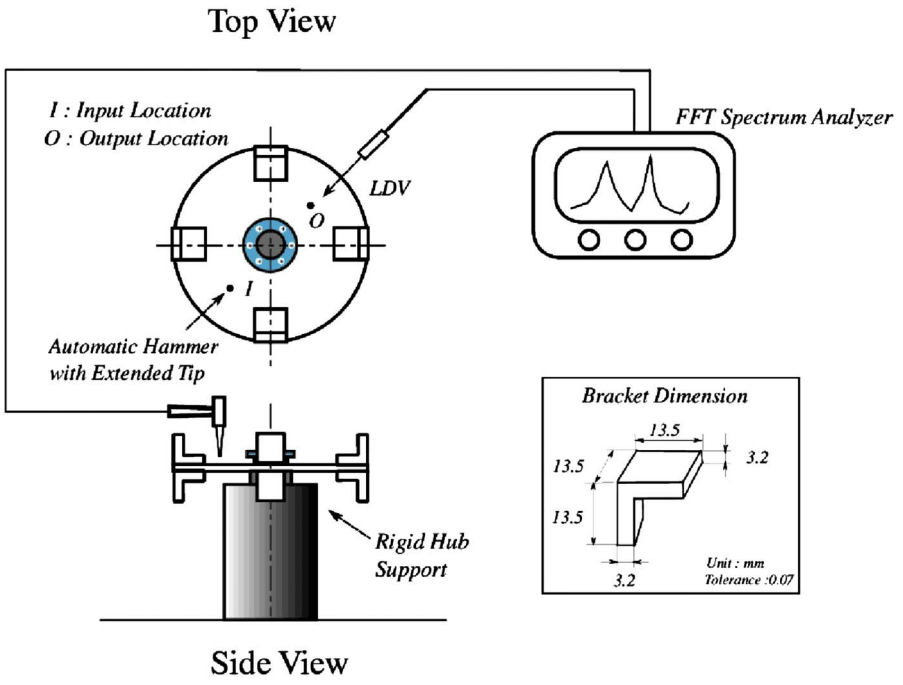

Fig. 5 Schematic of the experimental setup

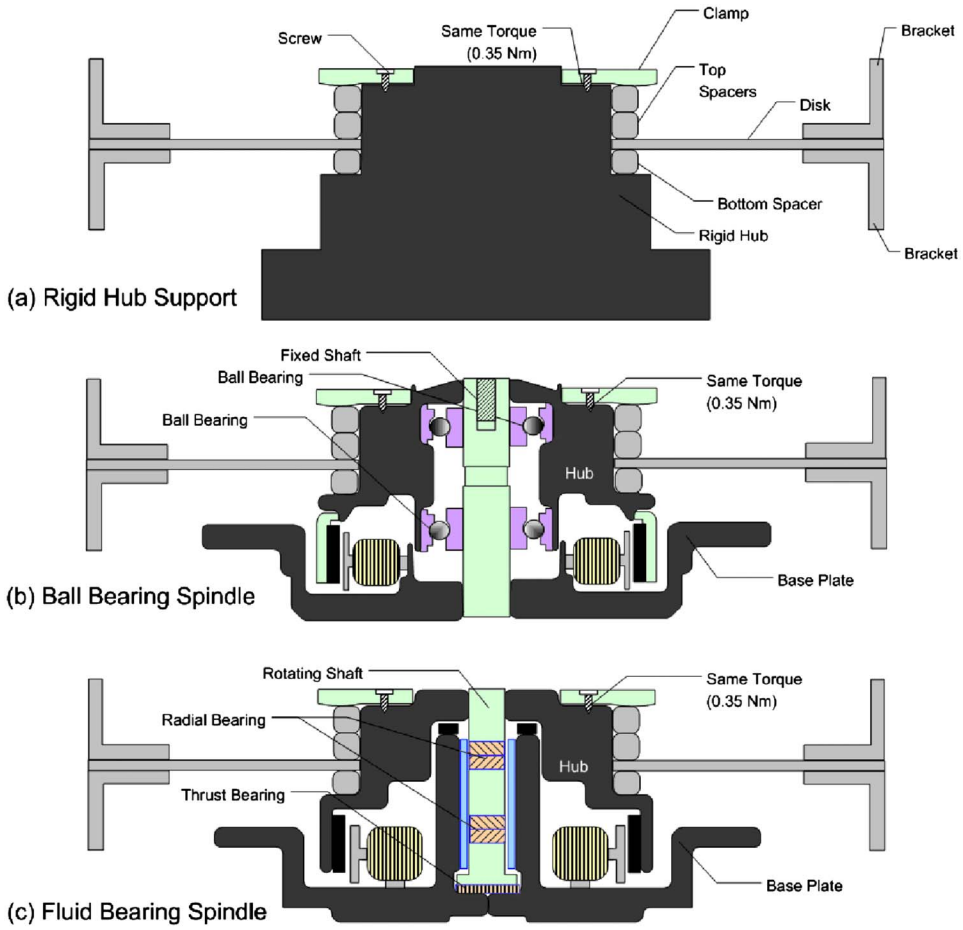

Fig. 6 Cross sections of rigid hub, ball-bearing motor, and fluid-dynamic bearing motor

Downloaded 11 Sep 2009 to 128.12.241.41. Redistribution subject to ASME license or copyright; see http://www.asme.org/terms/Terms_Use.cfm

Table 3 Natural frequencies (in Hz) measured from the stationary test

Mode	Rigid hub	BBS	FBS	% change (BBS)	% change (FBS)	Prediction
(0,1)	480.02	337.08	315.73	−29.8	−34.2	Unbalanced
(0,1)	484.87	342.5	N/A	−29.4	N/A	Unbalanced
(0,0)	509.04	506.59	513.21	−0.5	0.8	Unbalanced
(0,2)L	500.15	507.2	506.41	1.4	1.3	Balanced
(0,2)H	1038.82	1059.79	1055.55	2.0	1.6	Balanced
(0,3)	1492.79	1481.6	1229.61	−0.7	−17.6	Unbalanced
(0,3)	1497.9	1495.59	1286.44	−0.2	−14.1	Unbalanced
(0,4)L	2295.05	2301.32	2300.07	0.3	0.2	Balanced
(0,4)H	2425.21	2758.35	2387.07	13.7	−1.6	Unbalanced
10th	3124.01	3013.75	1976.36	−3.5	−36.7	Unbalanced
11th	3142	3039.99	1999.4	−3.2	−36.4	Unbalanced
12th	3390.46	3425.41	3415.71	1.0	0.7	Balanced
13th	3808.83	4092.63	4203.8	7.5	10.4	Unbalanced
14th	3986.02	3734.45	3494.72	−6.3	−12.3	Unbalanced
15th	3993.3	3762.3	N/A	−6.1	N/A	Unbalanced

spindle and the fluid-bearing spindle, respectively. The last column is the theoretical prediction of balanced and unbalanced mode from Table 1 for comparison.

From the results in Table 3, there are several issues worth noting. First, an unbalanced mode may experience a small frequency change for one housing while presenting a significant frequency change for the other housing. For example, the (0,3) modes undergo tiny frequency changes ($<1\%$) when the disk-bracket specimen is mounted on the ball-bearing spindle motor, but experience significant frequency changes when the disk-bracket specimen is mounted on the fluid-bearing spindle motor. The same phenomenon occurs for the 10th and 11th modes.

Second, all the predicted balanced modes, such as (0,2)L, (0,2)H, (0,4)L, and 12th modes, experience very small frequency changes ($<2\%$) in the experiments. Therefore, the theoretical predictions through nodal forces and moments in Eqs. (6) and (10) are valid criteria to identify balanced modes, and so is the prediction through phase index shown in Eq. (24).

Third, all the predicted unbalanced modes except one undergo significant frequency changes when the disk-bracket specimen is mounted on the ball-bearing or the fluid-bearing spindle. The only exception is (0,0) mode, whose natural frequency almost does not change for the ball-bearing or fluid-bearing spindle motors. This result, however, does not imply that the predictions in Eqs. (10) and (24) are inaccurate. As stated above, an unbalanced mode may not significantly change its natural frequency for a particular housing. For the (0,0) mode, it is likely that it is insensitive to both ball-bearing spindle and fluid-bearing spindle used in the experiments. In fact, Shen and Ku [10] showed that the (0,0) mode only experiences slight frequency changes when multiple disks are mounted onto a spindle. Moreover, the criteria in Eqs. (10) and (24) only predict the presence of balanced or unbalanced modes. The criteria do not predict the sensitivity or significance of the frequency changes.

6.2 Spinning Test. The disk-bracket rotor has also been tested at various spin speed to validate the existence of balanced modes as follows. The same experimental setup in Fig. 5 is used, except that the disk-bracket is mounted on a high-speed air-bearing spindle motor. The spectrum analyzer calculates the frequency response functions (FRFs) for various spin speeds to form waterfall plots, from which resonance frequencies are extracted to produce a Campbell diagram.

The disk-bracket rotor is then mounted on a hard disk drive spindle motor that employs oil-lubricated fluid-dynamic bearings. The same experiment is then repeated to obtain the Campbell diagram for various spin speeds. If a vibration mode is a balanced mode, it will not change its natural frequency when the disk-bracket rotor is switched from the air-bearing spindle to the hard disk drive spindle motor.

Figure 7 show the Campbell diagrams of the disk-bracket rotor mounted on the air-bearing spindle. For the air-bearing spindle, the disk-bracket assembly is mounted on the spindle via a bulky clamp simulating a fixed boundary condition. Therefore, we can use the finite element predictions in Figs. 3 and 4 to identify all the resonance branches according to the natural frequencies of the rotor at the zero spin speed. As shown in Fig. 7, some of the modes will split as the spindle spins but others do not. Those modes that do not split correspond to $\mathbf{A}_0(r,z) \neq \mathbf{0}$.

For the disk-bracket rotor tested, the periodicity $N=4$. Therefore, those modes, which do not split in Fig. 7, will have a phase index $n=4$ and $\mathbf{A}_0(r,z) \neq 0$ based on Table 2. According to Tables 1 and 2, balanced modes include (0,2)L, (0,2)H, (0,4)L, and the 12th mode. These balanced modes should not change their frequencies when the disk-bracket assembly is mounted onto the fluid-dynamic bearing spindle.

As a comparison, Fig. 8 shows the Campbell diagrams of the disk-bracket rotor mounted on the fluid-bearing spindle. There are several things worth noting. First, all the balanced modes, such as (0,2)L, (0,2)H, (0,4)L, and 12th mode, do not change their natural frequencies and mode splitting as predicted. Second, most of the unbalanced modes have significantly changed their natural frequencies, because the unbalanced modes have significant coupling between the disk-bracket assembly and the bearings of the spindle motor. As a result, it becomes difficult to trace the origin of each resonance branch for unbalanced modes. Third, (0,0) mode is an unbalanced mode, but it does not seem to change its natural frequency significantly when moved from the air-bearing spindle to the fluid-dynamic bearing spindle. This, however, does not imply that the prediction in the paper is wrong, because the theory can only predict whether or not a mode will shift its frequency. The theory, however, cannot predict how much a mode will shift the frequency. The frequency shift of an unbalanced mode highly depends on the stiffness of the bearings and the inertia of the rotor. According to our past experience [10], (0,0) mode tends to give very small frequency shift when mounted to a spindle motor.

7 Conclusions

In this paper, we consider a cyclic symmetric rotor having N identical substructures. In addition, each vibration mode of the cyclic symmetric rotor has a phase index $n \in (1,2,\ldots,N)$ satisfying Eq. (12). In addition, the vibration mode shape can be expanded into a Fourier series (13) in the circumferential direction,

Downloaded 11 Sep 2009 to 128.12.241.41. Redistribution subject to ASME license or copyright; see http://www.asme.org/terms/Terms_Use.cfm

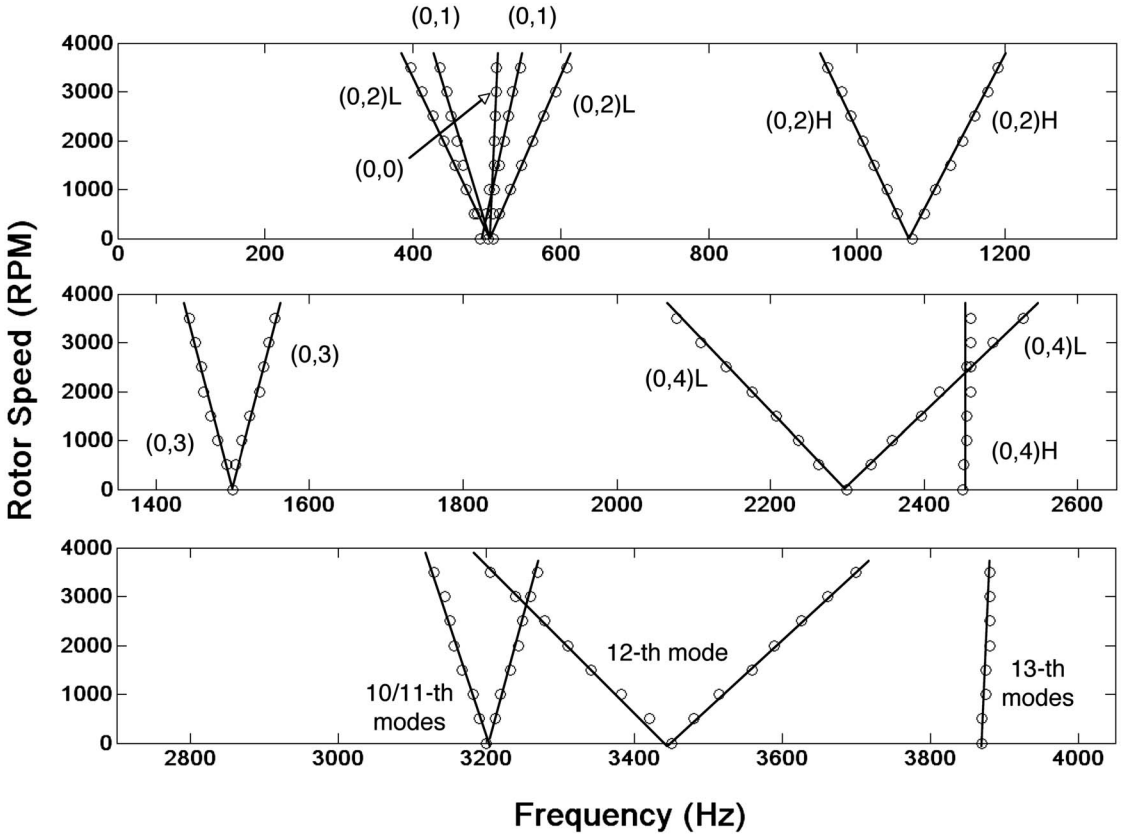

Fig. 7 Campbell diagram of the disk-bracket rotor on the air-bearing spindle

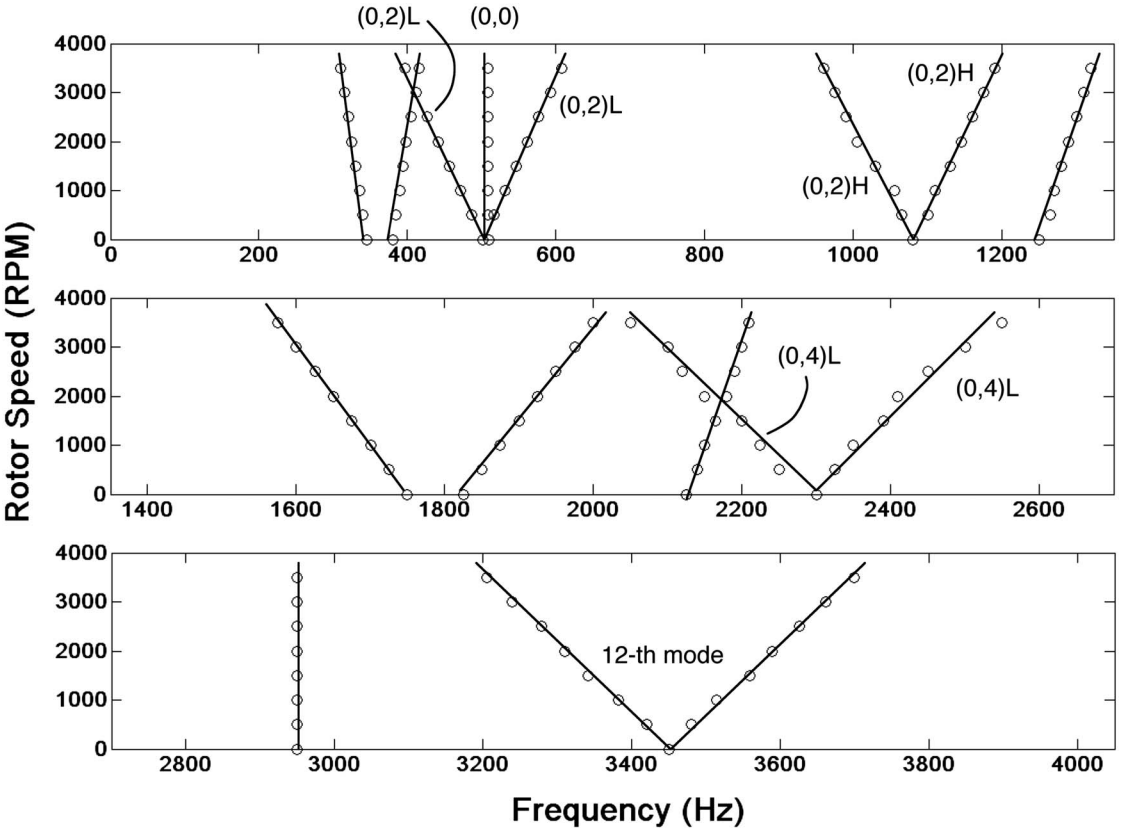

Fig. 8 Campbell diagram of the disk-bracket rotor on the fluid-dynamic bearing spindle

Downloaded 11 Sep 2009 to 128.12.241.41. Redistribution subject to ASME license or copyright; see http://www.asme.org/terms/Terms_Use.cfm

where $\mathbf{A}_k(r,z)$ are the corresponding Fourier coefficients. The theoretical analysis and experimental studies in this paper lead to the following conclusions.

(1) Before and after a rotor is assembled to a flexible housing via bearings, the vibration mode of the rotor may not change its natural frequency and mode shape. Such a mode is called a balanced mode, and its motion is decoupled from the housing and bearings.
(2) A balanced mode will have vanishing inertia forces and moments as it vibrates.
(3) If the rotor consists of a rigid portion and a flexible portion with the bearings located at the rigid portion, the condition of balanced modes is that the sum of the forces and the sum of the moments at the interface of the rigid and flexible portions shall vanish (see Eq. (10)).
(4) For a cyclic symmetric rotor with period N, a vibration mode will be a balanced mode if its phase index n satisfies $n \neq 1, N-1, N$. Moreover, for the case of $n=N$, the vibration mode will be a balanced mode if its leading Fourier coefficient $\mathbf{A}_0(r,z)=\mathbf{0}$.
(5) Experimental results show good agreement with the theoretical predictions.

References

[1] Chang, J. Y., and Wickert, J. A., 2001, "Response of Modulated Doublet Modes to Travelling Wave Excitation," J. Sound Vib., **242**, pp. 69–83.
[2] Chang, J. Y., and Wickert, J. A., 2002, "Measurement and Analysis of Modulated Doublet Mode Response in Mock Bladed Disks," J. Sound Vib., **250**, pp. 379–400.
[3] Thomas, D. L., 1979, "Dynamics of Rotationally Periodic Structures," Int. J. Numer. Methods Eng., **14**, pp. 81–102.
[4] Wildheim, J., 1981, "Excitation of Rotating Circumferentially Periodic Structures," J. Sound Vib., **75**, pp. 397–416.
[5] Wildheim, J., 1981, "Vibration of Rotating Circumferentially Periodic Structures," Q. J. Mech. Appl. Math., **34**, pp. 213–229.
[6] Tseng, J. G., and Wickert, J. A., 1994, "On the Vibration of Bolted Plate and Flange Assemblies," ASME J. Vibr. Acoust., **116**, pp. 468–473.
[7] Shen, I. Y., 1994, "Vibration of Rotationally Periodic Structures," J. Sound Vib., **172**, pp. 459–470.
[8] Tang, J., and Wang, K. W., 1999, "Vibration Control of Rotationally Periodic Structures Using Passive Piezoelectric Shunt Networks and Active Compensation," ASME J. Vibr. Acoust., **121**, pp. 379–390.
[9] Kim, H., and Shen, I. Y., 2009, "Ground-Based Vibration Response of a Spinning Cyclic Symmetric Rotor With Gyroscopic and Centrifugal Softening Effects," ASME J. Vibr. Acoust., **131**, in press.
[10] Shen, I. Y., and Ku, C. P. R., 1997, "A Nonclassical Vibration Analysis of a Multiple Rotating Disk and Spindle Assembly," ASME J. Appl. Mech., **64**, pp. 165–174.
[11] Childs, D. W., 1976, "Modal Transient Simulation—Modal for Flexible Asymmetric Rotors," ASME J. Eng. Ind., **98**, pp. 312–319.
[12] Genta, G., 1988, "Whirling of Unsymmetrical Rotors—A Finite Element Approach Based on Complex Coordinates," J. Sound Vib., **124**, pp. 27–53.
[13] Kang, Y., Shih, Y. P., and Lee, A. C., 1992, "Investigation on the Steady-State Responses of Asymmetric Rotors," ASME J. Vibr. Acoust., **114**, pp. 194–208.
[14] Chen, L. W., and Peng, W. K., 1997, "Stability Analyses of a Timoshenko Shaft With Dissimilar Lateral Moments of Inertia," J. Sound Vib., **207**, pp. 33–46.
[15] Ganesan, R., 2000, "Effects of Bearing and Shaft Asymmetries on the Instability of Rotors Operating at Near-Critical Speeds," Mech. Mach. Theory, **35**, pp. 737–752.
[16] Oncescu, F., Lakis, A. A., and Ostiguy, G., 2001, "Investigation of the Stability and Steady State Response of Asymmetric Rotors, Using Finite Element Formulation," J. Sound Vib., **245**, pp. 303–328.
[17] Raffa, F. A., and Vatta, F., 2001, "The Dynamic Stiffness Matrix of a Rotating Asymmetric Bernoulli–Euler Shaft," ASME J. Vibr. Acoust., **123**, pp. 408–411.
[18] Sekhar, A. S., and Srinivas, B. N., 2002, "Vibration Characteristics of Slotted Shafts," J. Sound Vib., **251**, pp. 621–630.

Downloaded 11 Sep 2009 to 128.12.241.41. Redistribution subject to ASME license or copyright; see http://www.asme.org/terms/Terms_Use.cfm